communications earth & environment

Article

https://doi.org/10.1038/s43247-024-01650-x

The local cooling potential of land restoration in Africa

Jessica Ruijsch [1] ✉, Adriaan J. Teuling [2] ✉, Gregory Duveiller [3] & Ronald W. A. Hutjes [1]

Land restoration is becoming increasingly popular as a climate change mitigation and adaptation measure. It is suggested that resulting vegetation changes can impact the local surface temperature through biophysical processes such as albedo warming and evaporative cooling. Yet, the potential effect of land restoration on the local surface temperature in Africa remains uncertain. In this study, we use Terra MODIS time series of vegetation, albedo, and land surface temperature to determine vegetation-temperature relationships at a continental scale. We show that vegetation-albedo and vegetation-temperature relationships do not only vary spatially across Africa but also temporally over different time scales, with strong cooling effects in semi-arid environments. Furthermore, we predict that land restoration can decrease local land surface temperature by around 0.2 Kelvin on average. This study gives a more detailed insight into where future land restoration provides additional positive climate impacts, and where land restoration may instead warm the local environment.

Land restoration practices, such as active reforestation, natural regeneration and water harvesting, have been proposed as a solution to a wide range of environmental problems across the world[1]. They have the potential to decrease and reverse land degradation, conserve biodiversity, and increase the livelihood of the local population through ecosystem services and income provision[2]. On top of that, planting trees is currently seen as one of the more realistic ways to sequester carbon, thereby compensating partly for the residual emissions that are hardest to decarbonize[3–6]. Consequently, land restoration efforts are becoming increasingly popular[7], including ambitious initiatives to plant millions of trees across the globe (e.g., the Bonn Challenge, the AFR100 project, and the Trillion Trees initiative). The African continent, even though having one of the lowest per-capita contributions to greenhouse gas emissions[8], is already experiencing an increase in temperature[9] and heatwave frequency[10] that is higher than the global average. This has resulted in biodiversity loss, droughts, reduced food production and economic growth, and loss of lives[11].

Land restoration may, in addition to global mitigation strategies, reduce the climate change impact in Africa[12]. Although it can encompass a wide range of measures and is implemented with different goals, land restoration often entails an increase in the greening of the surface[13] and can, therefore, directly affect the local climate through changes in the biophysical properties of the Earth's surface (e.g. albedo, evapotranspiration, and surface roughness). This way, land restoration projects have the potential to change the local and regional temperature[14,15] and create a more comfortable living environment for the local population[16]. Yet even though the scientific debate on how vegetation affects the regional climate started over 200 years ago[17], and the biogeophysical processes may sometimes be stronger than the biogeochemical ones[18], the biogeophysical processes and their related feedback have received much less attention.

When studying these vegetation–temperature relationships, it is, however, important to make a distinction between air temperature, which describes the ambient temperature of the air, usually measured at 2 m above a standard grass cover by weather stations; and land surface temperature, which is the radiative skin temperature of the Earth's surface as often measured by satellites. Although air temperature is an important variable because it can be directly felt by humans[16], mixing effects of surface fluxes in the boundary layer, in combination with limited data availability, make a continental analysis of vegetation–temperature interactions in Africa challenging. Land surface temperature, on the other hand, is available on a continuous grid throughout Africa by remote sensing data (e.g. MODIS land surface temperature[19]). In addition, although having a larger variation than the air temperature, the surface temperature is closely coupled to the Earth's energy balance and biophysical effects of vegetation changes, which makes it an ideal variable to study vegetation–temperature interactions.

Vegetation can directly affect the local surface temperature through multiple biophysical processes that amplify or counteract each other. For example, since highly vegetated areas are usually less reflective than bare land, the surface albedo in the visible range of the spectrum decreases with increasing vegetation cover. This results in a lower surface reflectance and a higher amount of net available energy, which therefore contributes towards

[1]Earth Systems and Global Change Group, Wageningen University and Research, Wageningen, The Netherlands. [2]Hydrology and Environmental Hydraulics Group, Wageningen University and Research, Wageningen, The Netherlands. [3]Max Planck Institute for Biogeochemistry, Jena, Germany.
✉e-mail: jessica.ruijsch@wur.nl; ryan.teuling@wur.nl

the warming of the surface and an increase in surface temperature[20,21]. This effect is often referred to as albedo warming. At the same time, an increased vegetation cover will result in a higher latent heat flux through evapotranspiration, contributing to the cooling of the Earth's surface by a decrease in sensible heat flux[22,23]. This process is often called evaporative cooling. Unlike albedo warming, which warms the earth as a system, the cooling due to evapotranspiration is local, and the heat is released upon condensation elsewhere. In addition, an increased surface roughness reduces aerodynamic resistance and therefore, increases turbulent energy flux dissipation, which also contributes to surface cooling[24,25].

Next to albedo warming and evaporative cooling, vegetation can also have more indirect effects on the surface temperature. The increased evapotranspiration, in combination with higher surface roughness, can increase atmospheric water vapour, causing an increased cloud cover and planetary albedo. This reduces incoming shortwave radiation and surface temperature[26,27]. At the same time, clouds can increase longwave radiation entrapment and, therefore, the surface temperature. Whether increases in vegetation cover and, thus, land restoration, result in a net surface warming or cooling depends on the relative importance of these direct and indirect processes[15,22], which appear to depend strongly on latitude[28,29], background climate[30], scale[26] and atmospheric conditions[31]. This makes it difficult to transfer results found in specific case studies to other areas. In addition, modelling studies also suggest non-local effects of vegetation cover on the surface temperature due to changes in large-scale circulation and atmospheric feedbacks that are difficult to capture with observational data[32,33].

As a result, it is largely unknown if land restoration, by increasing vegetation, can be used to reduce local surface temperatures in Africa through biophysical processes, and how large this temperature reduction is. To reduce this knowledge gap, previous studies have investigated the relationships between vegetation cover change and temperature on continental or global scales using modelling as well as remote sensing data[28]. However, many of these studies specifically focus on forests using idealized

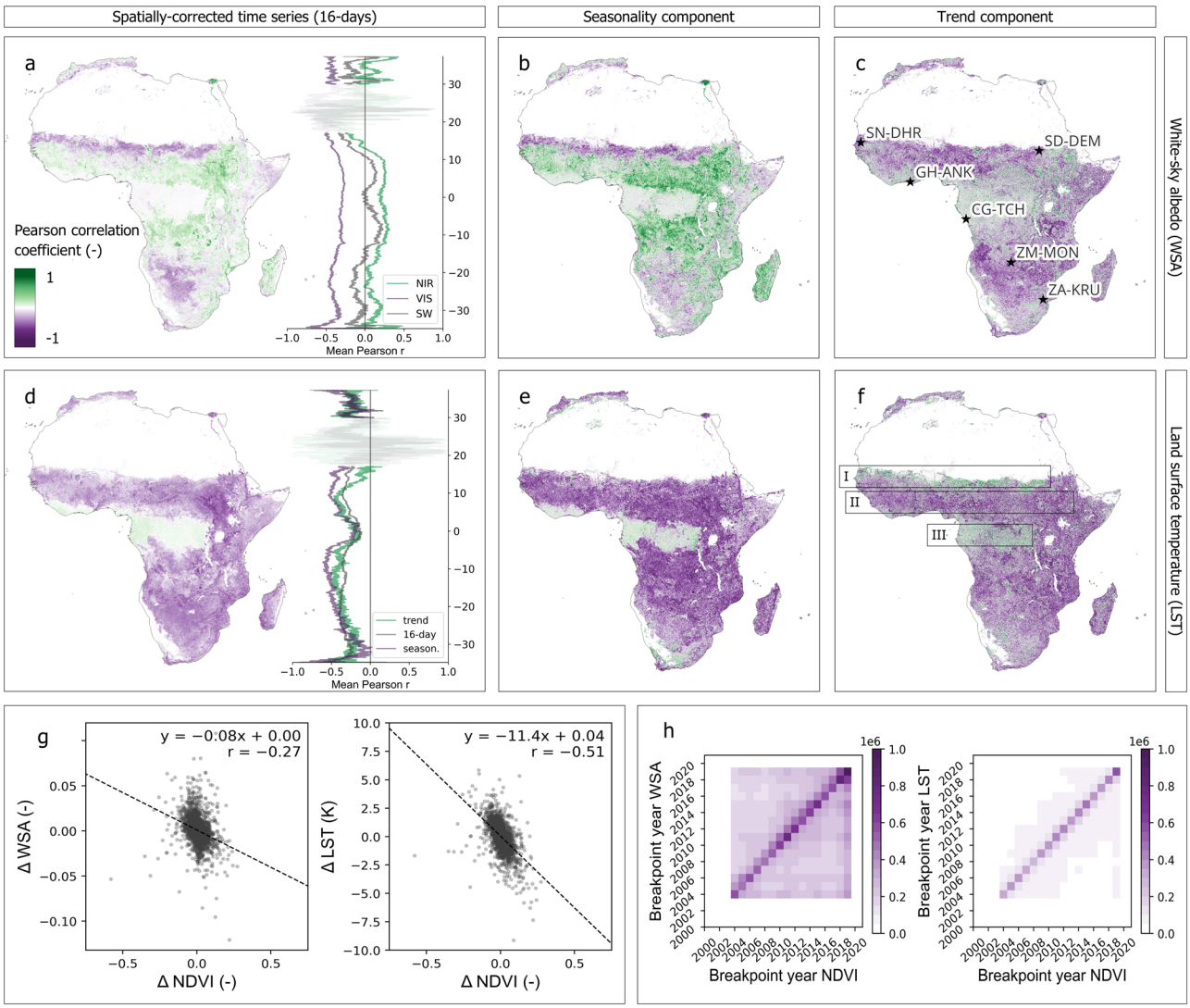

Fig. 1 | Sensitivity of white-sky albedo and land surface temperature to vegetation. Spatial distribution of the correlation between spatially corrected NDVI and spatially corrected shortwave broadband white-sky albedo (WSA) on either **a** the standard 16-day times series, **b** the seasonal component only or **c** the trend component. The line graph in **a** shows the mean 16-day correlation coefficient per degrees latitude for the shortwave (SW), visible (VIS) and near-infrared (NIR) WSA. Due to the limited data availability, the graph is masked between 17°N and 30°N. **d**–**f** Similar for the land surface temperature (LST), but the line graph in **d** shows the mean correlation coefficient per degree latitude for the 16-day, seasonality, and trend component. **g** Median spatially corrected NDVI, shortwave WSA and LST over the study period at 3183 randomly selected points. The line shows the linear fit of the points. **h** Distribution of year of breakpoint for 16-day NDVI, WSA and LST in the study area. Only pixels where both variables show a breakpoint are included, containing 22% and 7% of the pixels for the WSA and LST, respectively. In the figures, areas with a median NDVI lower than 0.15 or a non-significant correlation ($p > 0.05$) are not included. The boxes I, II, and III in **f** represent three exemplary regions in Africa with distinctive albedo-temperature–vegetation relations. The stars in **c** represent the locations of the EC-measurements in Fig. 3.

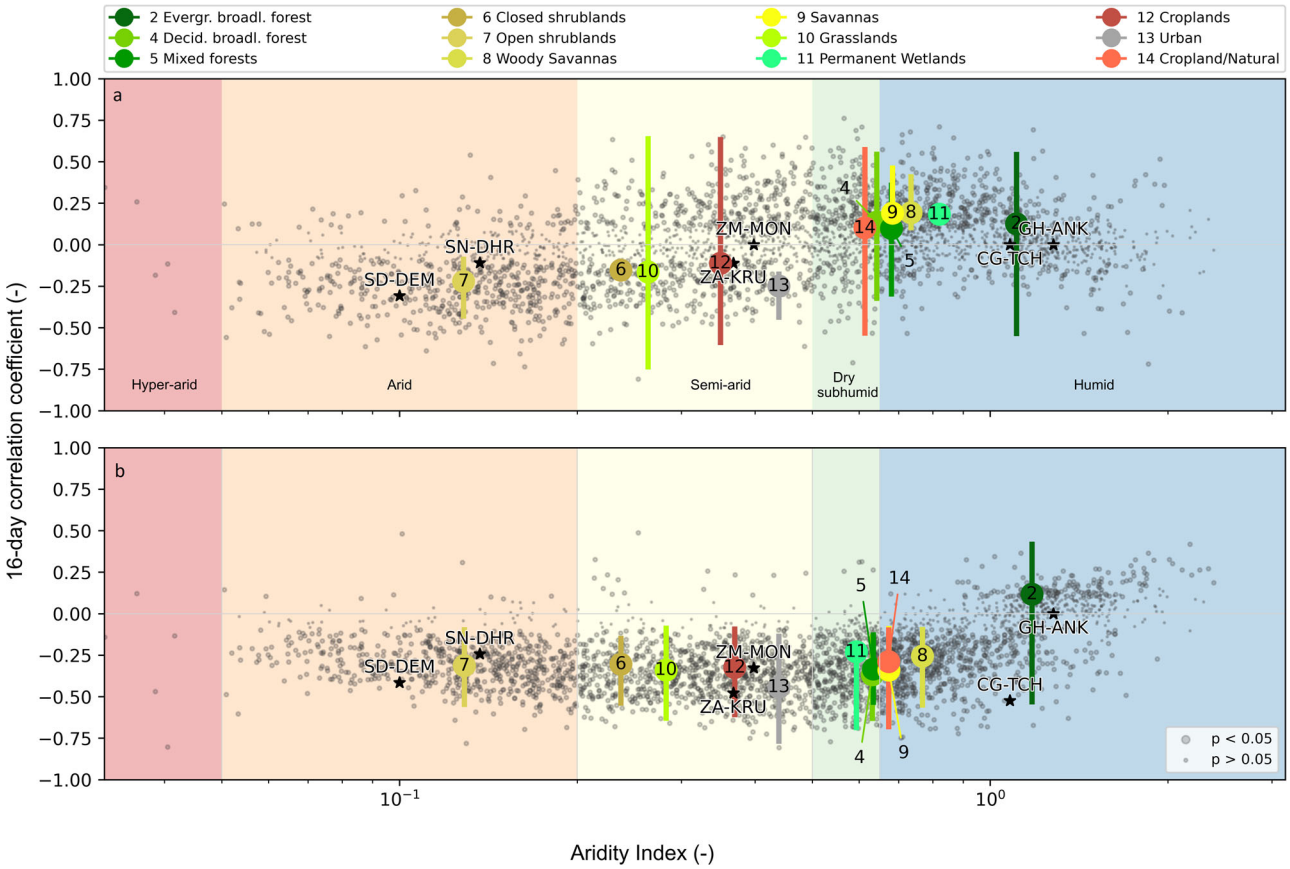

Fig. 2 | Land cover and aridity controls on vegetation–climate relationships. **a** Correlation coefficient of spatially corrected NDVI and shortwave White Sky Albedo (WSA) and **b** spatially corrected NDVI and land surface temperature (LST) over aridity index (scatter) and land cover classes (bars) based on 3183 random points inside the study area, with a median NDVI higher than 0.15. The points and vertical lines indicate, respectively, the median and interquartile range of the correlation coefficient per land cover class overall data. The horizontal position is determined by the median aridity index value of the respective land cover class. Only land cover classes that occur in the study area are included in this graph. In the scatter plot, non-significant correlations are marked with a smaller point ($p > 0.05$). In the land cover classes, non-significant correlations are not included. The stars represent the locations of the EC-measurements in Fig. 3.

afforestation scenarios or potential tree cover maps[5,34–36], while large parts of dryland Africa consist of savannas and grasslands. In these regions, land restoration-induced vegetation changes do not, and should not[37], necessarily result in a change in forest cover but rather increase the vegetation greenness by converting, for example, bare land to grasslands[13]. As these dryland areas may experience lower evaporative cooling due to their aridity, there is a need to include changes in dryland vegetation cover in these analyses. On top of that, little research has been done to predict the amount of local surface cooling that can be achieved through potential future land restoration practices of non-forested areas.

In this study, we aim to determine the direct local biophysical surface cooling effects of land restoration across Africa. Although land restoration is a broad concept and not all projects aim to increase vegetation cover, we follow the definition of the UNCCD[38], which includes both natural area conservation and sustainable land management of agricultural areas. For this reason, we expect restored areas generally to be associated with more natural ecosystems and a greener surface, including increases in grasslands or shrublands. In addition, we expect restoration-induced surface temperature changes mainly to be caused by changes in vegetation cover. To this end, we study the effect of increased vegetation greenness on the local surface temperature across the African continent. We apply a spatial-context method[13,39,40] to a time series of normalized difference vegetation index (NDVI) and land surface temperature (LST) obtained from the moderate-resolution imaging spectroradiometer (MODIS) on board the Terra platform, resulting in spatially corrected time series of these variables. In this method, we compare the time series at a given point with the average values of its surroundings. By doing so, we limit the effect of the natural climate variability, and we can thus demonstrate whether a pixel that is greener than its surroundings is also cooler. We also study the relationship between NDVI and white-sky albedo (WSA), as the albedo is an emergent property of the underlying vegetation, and it is also a driver of surface temperature. Combined with eddy-covariance data from six measurement sites, this allows us to explore relationships amongst the variables (NDVI-LST and NDVI-WSA) at both continental and case study scales for different aridity zones and land cover types. In addition, we use a data-driven approach to predict the direct local biophysical surface cooling or warming that could be achieved following greening due to large-scale land restoration in Africa. We recognize that not all small-scale greening is induced by land restoration[13], but we believe that by studying these vegetation–temperature relationships, we provide high-resolution information across multiple aridity zones on where land restoration projects can expect local biophysical surface cooling, and where they instead result in warming. This can guide policymakers in the design of future land restoration projects across Africa.

Results

Vegetation, albedo and surface temperature relationships across time scales

In order to reconcile previous studies, we analyse the vegetation–temperature relationships at three different time scales (see the "Methods" section). On a 16-day time scale (i.e., the original time scale of the input data), 31% of the study area shows a significantly negative correlation between the spatially corrected normalized difference vegetation index (NDVI) and spatially corrected shortwave white-sky albedo (WSA). Even though there is small-scale variability in correlations, we see clear large-scale

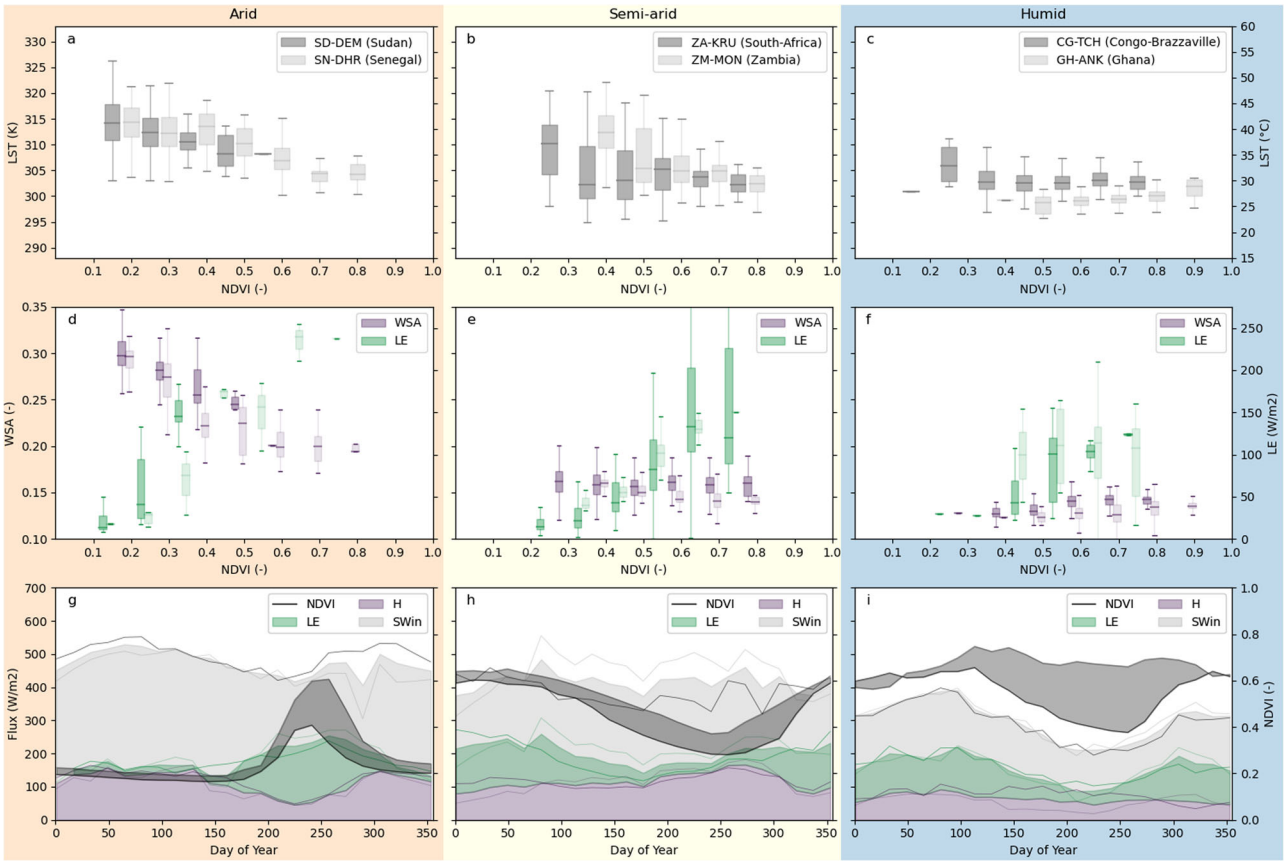

Fig. 3 | Aridity controls on vegetation–climate relationships from MODIS and eddy-covariance (EC) data. Relationships between NDVI and **a**–**c** LST, **d**–**f** WSA and **d**–**f** latent heat flux (LE) at six EC measurement sites (two per plot) across aridity classes. Plots show median (line), interquartile range (box) and data range with a maximum of 1.5 times interquartile range (whiskers). **g**–**i** Seasonality of the NDVI, latent heat flux (LE) (green area), sensible heat flux (H) (purple area) and difference between incoming shortwave radiation and sum of latent and sensible heat (SWin) at the same sites. The thin coloured lines (fluxes) and black shaded areas (NDVI) show the two sites separately. The locations of the sites are shown in Supplementary Fig. 1d. Measurements of NDVI, LST and WSA are obtained from not spatially corrected MODIS data, the net radiation, sensible heat flux and latent heat flux are obtained from EC measurements. Seasonality of the other variables at the six stations is included in Supplementary Fig. 14, showing a distinct seasonal variation in NDVI–WSA, NDVI–LST, NDVI–air temperature and NDVI–LE relations and a changing negative to positive correlations from arid to humid stations.

patterns, with negative NDVI–WSA correlations mainly in southern Africa and the Sahel area (Fig. 1a). This suggests that these areas experience a decrease in WSA (darker surface) compared to surrounding areas if the NDVI increases (more vegetation) compared to surrounding areas. Positive correlations between the NDVI and shortwave WSA cover 29% of the study area. As vegetation is usually considered less reflective (lower albedo) than bare land, positive NDVI–WSA correlations may appear counterintuitive. However, denser vegetation will also reflect more near-infrared light, thereby contributing to a positive relationship in that part of the spectrum. To elaborate on this effect, we applied a similar analysis separately to the visible broadband (0.3–0.7 μm) and near-infrared broadband (0.7–5.0 μm) WSA, which are both provided by the MODIS albedo products. This shows that the positive correlations in the shortwave broadband (0.3–5.0 μm) are mainly caused by the NIR broadband, as the visible broadband WSA is negatively correlated with NDVI across the study area, as could be expected (Fig. 1a, Supplementary Fig. 2).

Because previous studies have found contrasting biophysical vegetation–surface temperature relationships across time scales[24], we separate the 16-day time series into seasonal and long-term effects of vegetation cover changes using time series decomposition. This is especially relevant when determining the biophysical effects of land restoration, as these projects can affect the long-term greenness trends. Interestingly, contrasting spatial patterns in WSA–NDVI correlation appear for different time scales (Fig. 1b, c). Areas in subtropical Africa (delineated as box II in Fig. 1f) show, for example, a positive correlation on a seasonal scale, but a negative correlation across years (i.e., the trend component). Over the whole study period, the median spatially corrected NDVI and WSA values show a weak negative correlation with a correlation coefficient of –0.27 (Fig. 1g).

To further explore the relationship between vegetation and albedo, we compare the timing of breakpoints (i.e., significant and sudden changes in the trend component) and find that these moments often coincide, although sometimes the breakpoint in WSA is one year delayed (Fig. 1h). This suggests that sudden changes in NDVI trends are often followed by sudden changes in the WSA trend. Yet, in only 22% of the study area, a breakpoint is detected for both the NDVI and WSA. In 41% of the study area, no breakpoint is detected for both variables.

Similarly, on a 16-day time scale, NDVI and land surface temperature (LST) are significantly negatively related for 79% of the study area, suggesting an increase in NDVI (more vegetation) corresponds to a lower LST (cooler surface) compared to surrounding areas (Fig. 1d). In central Africa (box III in Fig. 1f), on the other hand, positive correlations occur. Similar patterns appear for the season and trend components of the time series (Fig. 1e, f). Only in the Sahel area (box I in Fig. 1f), do the trend components show a different result, with positive correlations between NDVI and LST, while the seasonal component shows negative correlations. Over the whole study period, the correlation between spatially-corrected NDVI and LST is negative, with a slope of –11.4 K (or −11.4 °C) and a correlation coefficient of –0.51 (Fig. 1g). In addition, the breakpoint year of the NDVI and LST

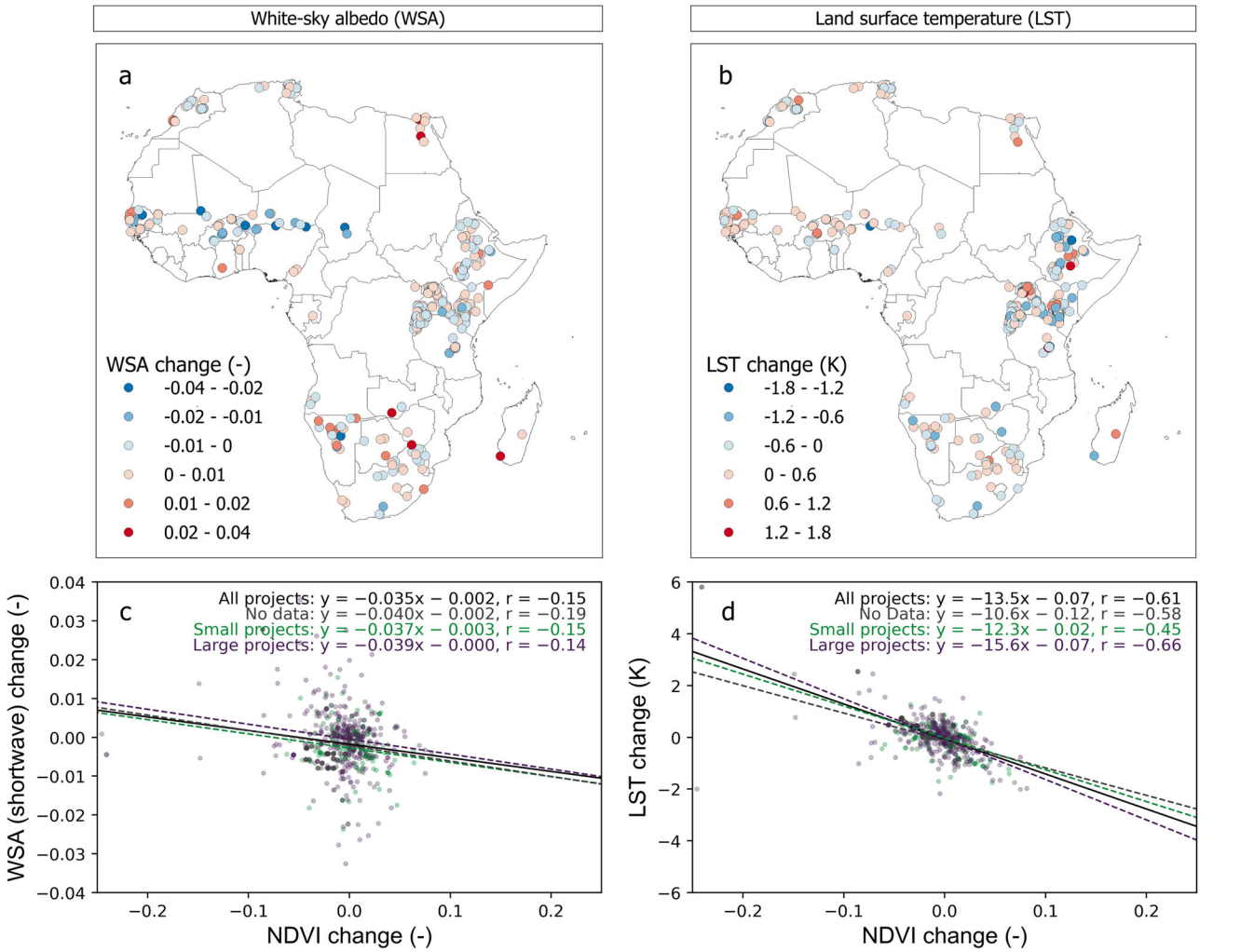

Fig. 4 | Observed climate impacts of local land restoration. Median change in the trend component of **a** the spatially corrected WSA and **b** LST in a 2000 m buffer around the WOCAT sustainable land management projects. The change is calculated as the last trend value of the study period minus the first trend value of the study period (i.e. $T_{2023\text{-}01\text{-}01} - T_{2001\text{-}01\text{-}01}$). Relationship between median change in trend component of **c** the NDVI and WSA and **d** the NDVI and LST for all projects (black), projects smaller than 1 km^2 (green; 24%), projects larger or equal to 1 km^2 (green; 37%) and projects that do not report a size (grey; 39%). The relationships for different types of sustainable land management projects are shown in Supplementary Fig. 15.

seem to coincide (Fig. 1h), suggesting that sudden trend changes in NDVI and LST occur simultaneously, although in 7% of the study area shows a breakpoint for both NDVI and LST and 58% does not show a breakpoint for both the NDVI and LST. Interestingly, in 33% of the study area, there is a breakpoint detected in the NDVI time series, but not in the LST time series. This suggests that the LST often changes more gradually, or other processes affect the LST from changing with the NDVI.

Effects of aridity and land cover

The biophysical effects of vegetation show clear spatial patterns related to both aridity and land cover. The negative 16-day correlations between NDVI and WSA often coincide with lower aridity index values (i.e., more arid environments), with increasing correlations over higher aridity index values (Fig. 2a). The highest (i.e., most positive) correlation coefficient values are found with an aridity index around 0.5, corresponding to semi-arid to dry subhumid environments. Towards more humid environments, the correlations between NDVI and WSA are low. A similar, but opposite pattern appears for the correlation value between NDVI and LST, as the correlation values decrease with the aridity index until an aridity index value of 0.5, and then increase again (Fig. 2b). However, for the most humid areas in Africa, the correlation between NDVI and LST is not zero, but slightly positive.

Besides aridity, land cover also affects the correlation values between NDVI and WSA, even though land cover and aridity are certainly related. Positive correlation can mostly be found in forested areas and savannas, while negative relationships are present in grasslands, shrublands, and barren lands (Fig. 2a). Most land cover classes show negative correlations between NDVI and LST (Fig. 2b), except for evergreen broadleaf forest. Although land cover thus seems to influence the direction of the correlations, both positive and negative correlations can often be found within single land cover classes.

To provide a more mechanistic insight into the vegetation–climate relationships, we extend our analysis with eddy-covariance (EC) data from six measurement sites across aridity zones in Africa. At these sites, the transport of heat, mass and momentum are measured at high frequency, providing data for incoming shortwave radiation (SW_{in}), latent heat flux (LE) and sensible heat flux (H). Although measuring only at a single location and long-time series are often not available, these EC-measurement sites provide more detailed information on the effect of vegetation on the energy balance at a seasonal scale.

These site measurements show that LE is positively correlated to NDVI in arid regions in Sudan and Senegal, suggesting higher evaporation during greener periods (Fig. 3d). At the same time, the NDVI and WSA are negatively correlated (Fig. 3d), resulting in a lower reflection of incoming

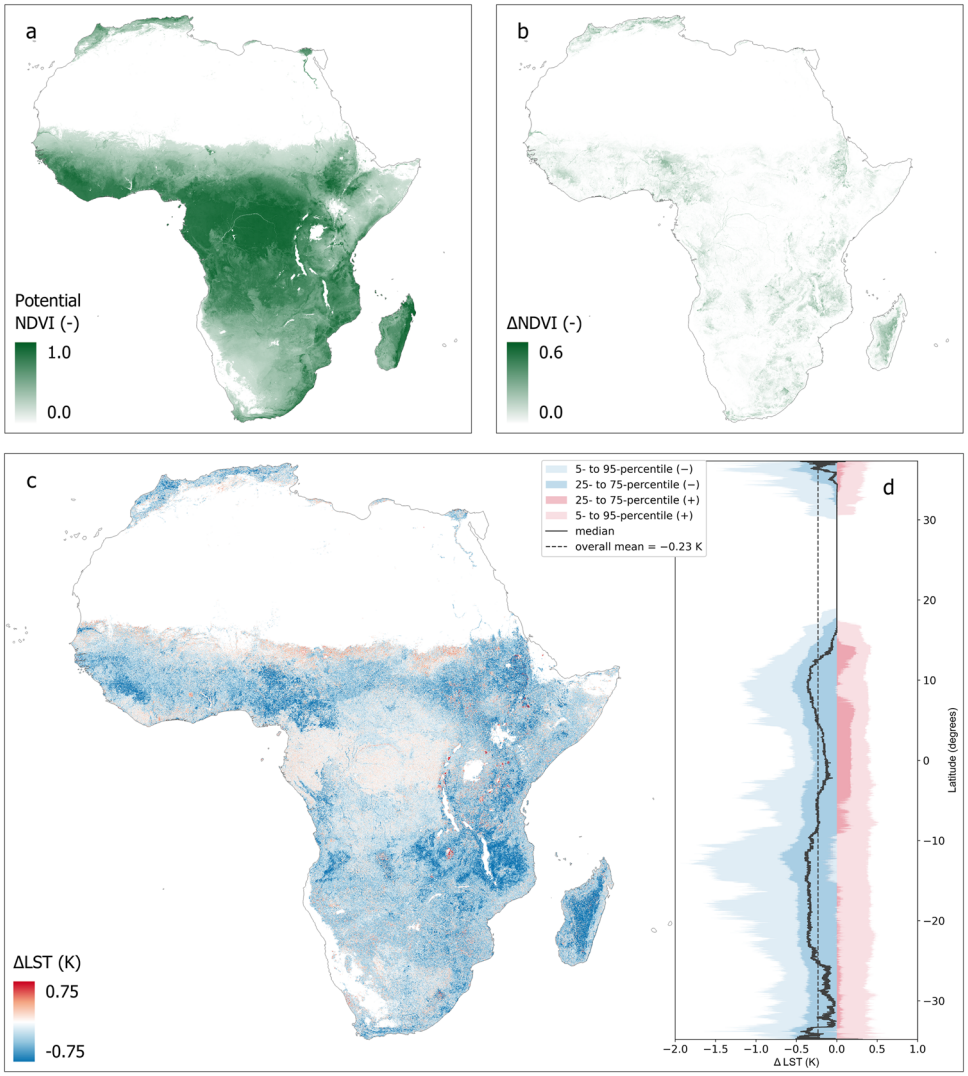

Fig. 5 | Potential local land surface temperature changes due to land restoration. a The potential NDVI obtainable by land restoration, predicted using maximum random forest regression and **b** the NDVI increase compared to the original median NDVI. **c** The potential local LST change obtainable by land restoration is predicted using random forest regression. For visualization purposes, the colour scale ranges from −0.75 to 0.75 K, containing 91% of the values. **d** The median and percentiles in ΔLST grouped by latitude. The overall mean indicates the mean potential change in surface area across the study area (excluding non-vegetated areas) of −0.23 K.

solar radiation, and a higher available radiation (represented by the sum of LE and H compared to SW_{in}) during periods of high NDVI (Fig. 3g). However, during these periods, the LE increases to such an extent, that we see a decrease in H during periods of the year with higher NDVI. This is consistent with the decreasing surface temperature during periods of high vegetation greenness measured with MODIS (Fig. 3a). In semi-arid regions, as represented by the sites in Zambia and South Africa, similar relationships to those in arid regions are observed (Fig. 3b, e, h), also suggesting a surface cooling effect of vegetation greening. However, NDVI–WSA relationships seem to be particularly weaker compared to arid regions. In addition, some other regions in northern Africa show positive NDVI–WSA correlations (Fig. 1b). Yet, the negative NDVI–H and NDVI–LST relationships suggest that also in these semi-arid regions, the increase in latent heat dominates the temperature signal of vegetation. In humid regions in Ghana and Congo-Brazzaville, on the other hand, an increasing NDVI does not have a large effect on LST (Fig. 3c) or H (Fig. 3i), even though the available radiation has a defined seasonality. In addition, the NDVI–WSA relationships seem to have a limited effect on the energy balance, represented by a constant sum of LE and H compared to SW_{in} throughout the year. The limited data availability of the MODIS data due to high cloud cover makes it, however, more difficult to interpret the energy balance.

Surface cooling effects of land restoration projects

To determine what the effect of implementing land restoration projects has been on the surface temperature, we compare the WSA and LST at project locations of 434 sustainable land management (SLM) projects in Africa. The median change in the trend component of WSA and LST over the study period (i.e., $T_{2023\text{-}01\text{-}01} - T_{2001\text{-}01\text{-}01}$) shows mixed results across the project locations, with both decreases and increases in WSA and LST without a clear spatial pattern (Fig. 4a, b). Yet, comparing the results to changes in NDVI, general negative NDVI–WSA and NDVI–LST relationships can be found for the SLM projects (Fig. 4c, d), although it should be mentioned that projects larger than the resolution of the data (1 km^2) show stronger NDVI–LST relationships. This suggests that both WSA and LST decrease with increasing NDVI and the spatial pattern in Fig. 4a, b results from variations in changing NDVI, or the effectiveness of regreening, at the project sites. Across Africa, greening at SLM projects thus generally seems to have a cooling effect on the land surface temperature, with the limited impact of albedo warming represented by the negative NDVI–WSA relationships. No particularly different relationships were found for different aridity zones. It should be noted that the concept of sustainable land management could be considered broader than the definition of land restoration provided by UNCCD[38]. Therefore, we included a similar analysis for separate SLM types in Supplementary Fig. 15, where the strongest NDVI–WSA correlations are found for revegetation and the strongest NDVI–LST correlations are found for agroforestry.

Local surface cooling potential of large-scale land restoration

By extrapolating on the relations found in this study, we can predict the local cooling effect of large-scale land restoration in Africa using a data-driven

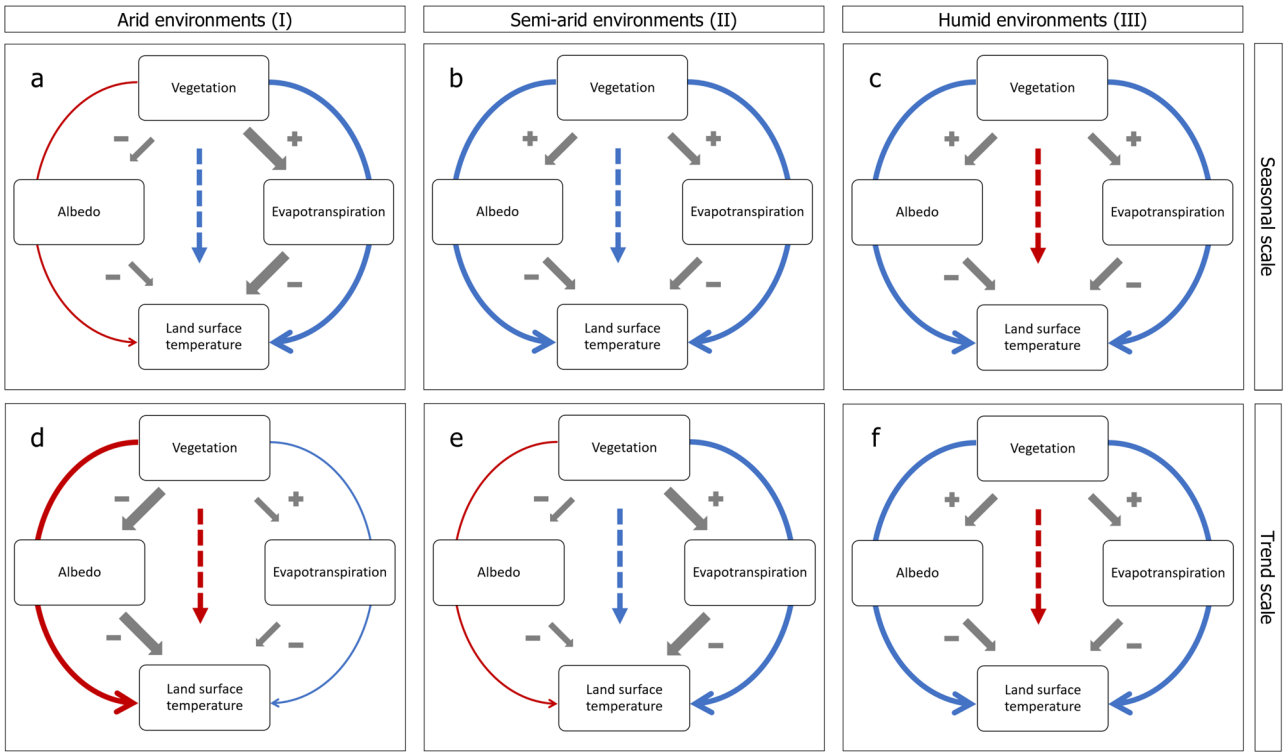

Fig. 6 | Perceptual model of vegetation–climate relationships. Vegetation–albedo and vegetation–temperature relationships in arid (**a**, **d**), semi-arid (**b**, **e**) and humid environments (**c**, **f**) in northern Africa on seasonal (**a**–**c**) and trend (**d**–**f**) time scales. The locations of arid, semi-arid and humid environments correspond to the boxes in Fig. 1f, annotated with respectively I, II and III. Positive relationships are indicated with a plus sign and negative relationships with a minus sign. The overall net albedo/evapotranspiration warming of potential vegetation increase is indicated with a red arrow, cooling with a blue arrow. The dotted arrows indicate the observed vegetation–temperature relationship, where a red arrow again suggests warming due to a vegetation increase and a blue arrow cooling. For all arrows, large arrows show the assumed dominant processes.

approach. As a first step, we determined the maximum potential NDVI constrained by aridity, surface temperature, elevation, slope, aspect, soil fertility and water table depth through maximum random forest regression (Fig. 5a). The difference between this potential NDVI and the current NDVI (ΔNDVIp) represents the NDVI increase obtainable by large scale land restoration initiatives. We can observe that the largest NDVI increases can be achieved in semi-arid regions. In the more humid areas in central Africa, as well as very dry areas, there is little potential for greening (Fig. 5b). It is important to note, however, that the potential NDVI increase is only constrained by climatological and environmental variables. Socio-economic constraints, which play less of a role in explaining vegetation potential than climatic variables[41], as well as the need for agricultural land or urban areas, are not considered.

To predict the potential LST change (ΔLST) corresponding to ΔNDVIp, we used a random forest regressor at each location based on observed values of ΔLST and ΔNDVI, and the aridity index, land cover class, median NDVI, median LST, median WSA, longitude, latitude, and elevation sampled at random locations. These observed values of ΔLST and ΔNDVI are obtained from the trend component rather than the seasonal changes to match the gradual increase in NDVI from land restoration. Using this regression model, large parts of Africa show cooling as a result of large-scale land restoration, with LST changes up to −4 K (Fig. 5c), although 98% of the study area shows a change between −1.5 and 1.5 K. In these areas, large-scale land restoration projects can result in a potential surface temperature decrease. However, the driest regions in the study area, such as in the Sahel and southern Africa, as well as humid areas, such as the rainforests of Congo, show a slight warming potential (Fig. 5d). The mean LST change over the whole study area, including regions with little potential for NDVI increases, is −0.2 K, suggesting an overall local cooling potential of large-scale land restoration in Africa (Fig. 5d). Yet, as we extrapolate measured relationships between the NDVI and LST, it should be noted that we can only predict the direct local effects of large-scale land restoration across Africa, while non-local or indirect climate effect through changes in atmospheric circulation is not included in this prediction. If all the suggested areas are restored at once on a large scale, different patterns may appear. These results can, however, be used to see where land restoration in Africa can cause local cooling, and where it instead may result in warming.

Discussion

In this study, we observed variations in vegetation–albedo and vegetation–surface temperature relationships across both spatial and temporal scales. However, before we discuss these in more detail, several uncertainties should be kept in mind when interpreting these results. Firstly, the use of image composites for land surface temperature results in a bias for clear-sky conditions, suggesting that the relationships we found related to LST are representative only for days without cloud cover. Clouds can have a considerable impact on the surface energy balance due to changes in incoming longwave and shortwave radiation[32]. Therefore, the year-round relationships between vegetation and surface temperature may deviate from the results found in this study. In addition, the land surface temperature values used in this study may be different from the air temperature measured by weather stations and often felt by humans[42], especially during dry seasons[42]. It is estimated that the effect of vegetation on land surface temperature is stronger than on air temperature, partly caused by the clear-sky bias of remotely sensed land surface temperature[43], which is also observed at the EC measurement locations (Supplementary Fig. 14). Also, the mixing of the boundary layer causes surface temperature effects to be more local than air temperature effects. We, therefore, expect the air-cooling effect of land

restoration projects to be smaller than the surface cooling as observed in this study, which should be taken into consideration while planning future land restoration projects. On the other hand, because satellite-derived surface temperature values are detected at the top of the canopy layer, the additional shade effects that vegetation can provide are not considered. In addition, also radiative heat emitted by the surface can be felt by humans. Similarly, the albedo is not only affected by changes in vegetation but also by soil background signals. This is especially relevant in arid regions with large fractions of bare ground. Furthermore, because wet soils have a lower albedo than dry soils, soil moisture content has a considerable impact on albedo in these areas[44,45]. In addition, the white-sky albedo only represents the bihemispheric reflectance, while the actual albedo value as measured on the ground (i.e., blue-sky albedo) also contains a directional hemispherical reflectance component (i.e., black-sky albedo). We are convinced that changing white-sky albedo to blue- or black-sky albedo would likely only have a very limited effect on the results. Furthermore, the overall accuracy of MODIS albedo is generally high and does not appear to depend on illumination and viewing angles[46,47], which is important when studying larger areas. In addition, as the land surface temperature is affected by both albedo warming and evaporative cooling, as shown by the eddy-covariance data, a continental scale analysis of evaporation would be informative. However, remotely sensed evaporation is often computed using empirical relations between NDVI and evaporation, making it difficult to study changes in NDVI and evaporation independently. Although also NDVI and WSA cannot be studied completely independently, because the variables are based on the same spectral bands, we believe that using these variables is more appropriate than computed evapotranspiration values. Therefore, combining observed values from remotely sensed data with modelling studies incorporating air temperature, evapotranspiration, blue-sky albedo and cloudy days may provide a complete picture of the cooling potential of land restoration in Africa.

As vegetation–surface temperature relationships vary across Africa, we discuss three zones with distinctive characteristics in more detail: arid environments in the Sahel (Fig. 1f, box I), semi-arid and dry subhumid environments in northern Africa (Fig. 1f, box II) and humid environments in central Africa (Fig. 1f, box III), creating a perceptual model of vegetation–climate relationships across Africa. The perceptual model can also be applied to regions in southern Africa, although the boundaries between positive and negative relationships are less sharp.

In arid environments such as the Sahel, the results showed negative vegetation–albedo correlations on a seasonal scale, increasing net radiation and energy available for heat generation. Yet, the positive vegetation–evaporation relationships cause an increasing latent heat flux that compensates for this increase in available energy. This leads to a decrease in sensible heat flux and evaporative cooling during periods in the year with high vegetation cover (Fig. 6a). Although the EC measurements are too short to accurately analyse changes in long-term changes in the energy balance, we can extend the same reasoning to the trend scale (Fig. 6d), where we observe positive vegetation–surface temperature relationships. Warming due to a decrease in albedo thus seems to outweigh the decrease in sensible heat flux due to evaporation. This suggests that enough water is available for evaporative cooling during the wetter periods in the year when vegetation cover is high, but there is insufficient water to sustain this evaporative cooling effect during an overall increase in vegetation cover, resulting in a dominant albedo warming on the trend scale. Similar results were found by Chen et al.[25] and Feldman et al.[24], who showed that the long-term relationship between leaf area index and land surface temperature is dominated by the albedo in this area, causing a warming effect of vegetation increases.

In semi-arid and dry subhumid environments in northern Africa, vegetation variations are positively correlated to the albedo on seasonal time scales, indicating more reflectance with higher vegetation covers (Fig. 6b). Although this may seem counterintuitive as vegetated surfaces are usually considered darker due to the absorption of visible (VIS) radiation, a distinctive property of vegetation is the high reflectivity of radiation in the near-infrared (NIR) range[48] (Supplementary Fig. 2). Since both the NIR and VIS range are included in the white-sky albedo[49], a dominant increase in the reflection in the NIR range over a decrease in the reflection in the VIS range can explain the positive vegetation-albedo correlation. Previous research estimated the vegetation–albedo relationship to be highly variable and depending on location[50], where positive relationships between vegetation and NIR albedo were found, especially in the growing season[51–53]. Together with the fact that albedo can be positively related to leaf area index, but negatively to forest cover[50], this can explain the difference between the seasonal and trend vegetation-albedo correlations found in this study (Fig. 6e). In addition, dryland Africa is a hotspot for fires, where some regions burn almost every year[54]. The coincidence of the resulting decrease in albedo[55,56] and vegetation cover caused by the fires can explain the positive seasonal-scale albedo–vegetation relationships in these areas. In some semi-arid regions in southern Africa, on the other hand, vegetation and albedo are negatively correlated and EC measurements behave more as arid regions in northern Africa. Yet overall, we see a net cooling effect of vegetation on both the seasonal and trend scales in these semi-arid and dry subhumid areas, represented by the negative vegetation–surface temperature relationships, which may be caused by both a higher reflectance of near-infrared radiation on the seasonal scale, and evaporative cooling on the seasonal and trend scales.

Tropical forests and humid areas in central Africa, on the other hand, showed low, yet positive vegetation–surface temperature relationships on both the seasonal and trend scale, suggesting that an increase in forest cover would cause warming of the Earth's surface (Fig. 6c and f). This contradicts expectations, as tropical forests have a high evapotranspiration potential throughout the year and vegetation and latent heat flux are positively correlated. Combined with generally low vegetation–albedo correlation, a cooling effect would be expected[21], as predicted by many modelling and observational studies[57–59]. Yet, several studies using satellite-based vegetation and temperature data show a similar weak or slightly positive vegetation–albedo relationship in the tropical forests of central Africa[24,25,43]. In addition, satellite data estimations that deforestation in the Congo basin (i.e., a change from forests to grasslands) may potentially result in an increase in latent heat flux and a decrease in sensible heat flux. This would then cause a decrease in surface temperature and positive vegetation–surface temperature relationships[36,60]. Literature addressing this difference between different observational datasets and model results in tropical areas like Central Africa suggests the high cloud cover and the saturation of NDVI under high vegetation cover as potential causes[24]. Indeed, visual inspection of the NDVI time series reveals a large amount of noise (Supplementary Fig. 16), although using the enhanced vegetation index (EVI) or leaf area index (LAI), which are less sensitive to this saturation effect[61], does not result in substantial different spatial patterns (Supplementary Figs. 17 and 18). In addition, it should be noted that these humid regions are often energy-limited, rather than water-limited. This effect is distinctly visible in the EC measurements, as an increase in incoming shortwave radiation directly leads to increased evapotranspiration while the sensible heat remains constant. This could explain the weak correlations between vegetation and surface temperature in this study. However, considering the clear-sky bias and the overall low correlations found in these areas, we argue that the warming effect of reforestation in humid areas should be handled with care, and more observational data is needed to provide a complete explanation.

If we look in more detail at sustainable land management projects, no clear patterns in white-sky albedo and land surface temperature changes could be observed. This indicates that sustainable land management, in general, does not directly cause a cooling effect in Africa. This may partly be caused by the uncertainty related to the location and size of the WOCAT projects used in this study, as 27% of the projects are reported to be <1 km^2 and 38% did not report a size, and the absence of greening at some locations. In addition, it should be noted that the use of our spatial context method results in the detection of small-scale deviations in vegetation, albedo and temperature. In addition to land management, other small-scale processes, such as changes in the extent of surface water, irrigation and especially the

distribution of water, can cause variations in vegetation–surface temperature relationships[13]. Yet, comparing the changes in surface temperature with changes in NDVI, a clear negative relationship suggests that warming at the project locations is often due to a decrease in vegetation over time rather than the absence of a cooling effect of greening. Some projects that showed considerable greening resulted in a cooling of almost 2 K, suggesting that if the SLM projects result in greening, a cooling effect can often be expected.

Extrapolating the relationships found in this study to a large-scale restoration scenario, large parts of Africa, especially semi-arid environments, may experience local cooling under future land restoration, assuming enough water is available to sustain the increased evapotranspiration. Across Africa, we estimate that the potential land restoration can decrease the local surface temperature on average by 0.2 K, which is considerable in comparison to the projected mid-century temperature change between 0.5 and 2.5 K[9]. From a temperature perspective, a widespread increase in vegetation cover may, therefore, be beneficial in these areas. In addition, comparing the results of this study with the locations of existing land restoration projects, we expect a cooling effect of vegetation increases in large parts of projects such as the participating countries of the Great Green Wall of Africa[62]. However, some of these projects implemented in the driest regions, including parts of the Great Green Wall project, may experience biophysical warming due to a lack of moisture available for the increased evaporation. The contradicting vegetation–surface temperature relationships across time scales highlight the need to include both interannual as well as seasonal analyses before implementing land restoration projects. Furthermore, it should be kept in mind that we only determined the effect on land surface temperature in this study, while large-scale land restoration may have many other benefits as well as potential disadvantages related to biodiversity, social–economic aspects, and land use change[63]. In addition, land restoration does not only alter the energy balance through biophysical processes but can also affect the water cycle through changes in evapotranspiration, soil moisture and even precipitation[35]. On top of that, unexpected climate effects may appear outside the restored area, even if the restored area itself is cooling[32,57]. These effects are not included in this study. We, therefore, argue that a more complete picture of these different potential climate effects of land restoration is needed before large-scale land restoration is implemented. In this research, we do, however, provide some first guidance on where future land restoration could result in cooling, and where it instead shows warming.

Methods

Input data and pre-processing

In this study, we used five main datasets. The calculations were mostly done in Google Earth Engine[64]. To detect changes in vegetation cover, we used normalized difference vegetation index (NDVI) data from the terra moderate resolution imaging spectroradiometer (MODIS) Vegetation Indices Collection 6 dataset (MOD13Q1.061)[65] (Supplementary Fig. 1a). This dataset contains 16-day maximum value composites of NDVI at a 250 m resolution. The images were atmospherically corrected and masked for water, clouds, aerosols, and cloud shadows, using the provided quality indicators. For this analysis, images between 2001/01/01 and 2023/01/01 on the African content were used. Although the NDVI dataset has a 250 m resolution, we performed the analysis on a 1 km spatial resolution to match the land surface temperature data (using nearest-neighbour resampling to ensure fast computation). In addition, we masked areas with a median NDVI lower than 0.15, because of their low or absent vegetation cover. The masked areas are mostly located in the Sahara Desert and account for 36% of the African continent. It should be noted that this threshold is calculated on a 1 km spatial resolution, including small regions of high vegetation cover in the desert areas.

We studied the land surface albedo from the Terra and Aqua MODIS Albedo dataset (MCD43A3.006)[66], using white-sky (bi-hemispherical) albedo (WSA) (Supplementary Fig. 1c). The data is available on a daily time scale representing the 16 days around the central daily value. To match the NDVI data, we sampled the WSA data at the centre day of the NDVI 16-day periods generating 16-day WSA data. The main analysis was performed using the shortwave broadband range albedo (0.3–5.0 μm), containing both visible and near-infrared radiation, but a comparison to the visible broadband albedo (0.3–0.7 μm) and near-infrared broadband albedo (0.7–5.0 μm) is included in Supplementary Fig. 2. Note that the near-infrared spectral range of 0.7–5.0 μm is larger than the commonly used range and technically also contains shortwave-infrared. Although the WSA has a 500 m spatial resolution, calculations were done at a 1000 m resolution to match the LST data (using nearest-neighbour resampling). Again, areas with a median NDVI lower than 0.15 were masked.

Changes in surface temperature were detected using land surface temperature (LST) data from the terra MODIS land surface temperature and emissivity dataset (MOD11A1.061)[19] (Supplementary Fig. 1b), containing average LST data on a daily time step and a 1 km spatial resolution at an overpass time of 10:30 a.m. We used daytime land surface temperature values because we expected the effects of vegetation changes to be higher during the daytime. Although Aqua MODIS data (MYD11A1.061) has an overpass time of 1:30 p.m., which is closer to the expected highest daily temperature, we used Terra MODIS in this study due to the longer data availability. However, we explored the results of the different overpass times of the sensors in Supplementary Fig. 3. In addition, we included a sensitivity analysis of the results in the used LST algorithm (i.e., MOD11A1.061 vs. MOD21A1.061) in Supplementary Fig. 4. Both datasets showed similar spatial patterns on the continental scale. To match the temporal resolution of the NDVI data, the LST was downscaled to a 16-day temporal resolution by taking the median LST value over the 16-day period of the NDVI data, to represent the whole 16-day period. Supplementary Figs. 5 and 6 investigate different LST downscaling methods, showing variation in correlation strength but similar spatial patterns. Again, the areas with a median NDVI lower than 0.15 were masked.

Land cover data was retrieved from the MODIS Land Cover Type Collection 6 dataset (MCD12Q1), created using a supervised classification of the Terra MODIS and Aqua reflectance data[67] (Supplementary Fig. 1f). For this study, we used data from 2001 at a 500 m spatial resolution, representing the original land use at the start of the study period.

The aridity index (AI)[68] can be defined as the 30-year average fraction of precipitation and potential evapotranspiration. We used Aridity Index data from Zomer et al.[69], calculated over the 1970–2000 period on a 30-arcsecond resolution (Supplementary Fig. 1e). We then defined hyper-arid, arid, semi-arid, dry subhumid and humid areas as having aridity index values of $AI < 0.05$, $0.05 \le AI \le 0.2$, $0.2 \le AI \le 0.5$, $0.5 \le AI \le 0.65$ and $AI > 0.65$, respectively[70].

Spatial-context approach

Changes in WSA and LST are not only caused by changes in NDVI but also by large-scale background trends such as natural climate variability and global climate change. We corrected these background trends using a spatial-context approach[13,39,40]. In this approach, we assumed that natural climate variability acts on a larger scale than land restoration processes. Therefore, we could remove the background trend from a time series by subtracting the time series average over a neighbourhood around a pixel from the original time series. We called the resulting time series the spatially corrected time series (Supplementary Fig. 7). The neighbourhood is square-shaped with a radius of 25 km, corresponding to an area of 50 by 50 km. The centre of the neighbourhood with a radius of 1 km was not included in the neighbourhood average. We applied this method to each pixel in the study area, resulting in spatially corrected NDVI, WSA and LST time series. Using this approach, we could thus determine to what extent areas that are greener than surrounding areas are also cooler or warmer than surrounding areas. The size was based on Ruijsch et al.[13] and is a compromise between a larger area, but also remaining within similar aridity areas. A sensitivity analysis of the used neighbourhood size is included in Supplementary Fig. 8, showing lower correlations for smaller neighbourhood areas. A comparison of the corrected and uncorrected time series, which include large-scale natural variability, is included in Supplementary Figs. 9 and 10.

BFAST algorithm and breakpoints

Sometimes, land restoration can cause a detectable change in the ongoing trend of NDVI, WSA and LST time series. In addition, spatially corrected time series contain changes due to both seasonality and trend components, due to which simple linear regression does not provide sufficient information. To this end, we applied the breaks for additive seasonal and trends (BFAST) algorithm[71–73] in Google Earth Engine[74] (Supplementary Fig. 7). This algorithm separates a time series into a seasonality, trend and remainder component and can detect significant changes in the trend and seasonal component (i.e., breakpoints). We applied the BFAST algorithm to the spatially corrected NDVI, WSA and LST time series. We used the BFAST algorithm on each pixel in the study area with a seasonal harmonic model order of 3, the maximum number of breakpoints to 1 and minimum spacing between two breakpoints to 0.15, which is the fraction of the total time series length (i.e., 3 years). These settings were chosen to match the vegetation changes after land restoration (by including breakpoints) while limiting computation time (by limiting the number of breakpoints and seasonal harmonic model order)[13].

Correlations between NDVI, Albedo and LST

To provide insight into the relationships between NDVI, WSA and LST, we calculated the Pearson correlations coefficient between spatially-corrected NDVI and spatially corrected WSA, as well as between spatially-corrected NDVI and spatially corrected LST (results for the Spearman's rank correlation are included in Supplementary Fig. 11 to study nonlinear relations). We defined statistically significant values as having a p-value lower than 0.05. First, we compared for each pixel the 16-day average spatially corrected NDVI, WSA and LST, resulting in two correlation values over time for each pixel in the study area. This way, we can visualize spatial patterns in correlations. To distinguish how different time scales contribute to this correlation, we also calculated the correlation values for the seasonal and trend components of these 16-day time series. Next, we calculated the 20-year average spatially corrected NDVI, WSA and LST, after which we calculated the correlations over the whole study area. In addition, we compared the timing of breakpoints in the trend component as calculated by the BFAST algorithm. This allowed us to determine whether changes in NDVI directly result in changes in WSA and LST, or if there is a delay. Finally, we compared the found correlations with aridity index and land cover values to gain more insight into what causes spatial variations.

Eddy-covariance measurements

We used eddy-covariance measurements across Africa to provide more field-measured insights into the underlying relations of the remotely sensed data. The measurements are obtained from six stations in different aridity zones from the FLUXNET database in Sudan[75], Senegal[76], South Africa[77], Zambia[78], Congo-Brazzaville[78] and Ghana[79]. Detailed information on each station is available in Supplementary Table 1. The hourly sensible heat flux (H), latent heat flux (LE) and incoming shortwave radiation (SW_{in}) are matched to the MODIS data by taking the average value over each 16-day period. Only daytime values are used. In addition, because a comparison to surrounding areas is not possible with the EC measurements, we compare H, LE and SW_{in} to uncorrected (i.e., not spatially corrected) MODIS data. Due to limited data availability, we used mean NDVI, LST and WSA of an area of 10 km around the stations Congo-Brazzaville and Ghana. For the other stations, we used the data from the specific grid cell corresponding to the station location.

Sustainable land management projects

Next, we compared the results to existing land restoration projects to determine how land restoration affects local surface temperatures. To this end, we used 434 sustainable land management (SLM) projects in Africa from the World Overview of Conservation Approaches and Technologies (WOCAT)[80], downloaded from the Food and Agricultural Organisation of the United Nations (FAO) database. This dataset contains point locations with the locations of sustainable land management projects, ranging from tree planting to area closure and sustainable agriculture. As with the NDVI, we removed projects in areas with an NDVI lower than 0.15. Furthermore, as some projects consist of multiple locations, we split the projects into individual points, resulting in 628 project locations (Supplementary Fig. 1d). In addition, since the projects only contain point coordinates, we created a buffer area around each project point with a radius of 2000 m. For each of these buffer areas, we calculated the mean NDVI, WSA and LST to determine the NDVI–WSA and NDVI–LST relationship at sustainable land management projects in Africa. In addition, we calculated the actual changes in LST and WSA at the project locations, defined as the difference in trend component between the end and the beginning of the study period.

Predicting local biophysical cooling/warming due to land restoration

As a final step, we predicted the amount of local biophysical cooling or warming that can be achieved due to large-scale land restoration in Africa in two steps: (1) we calculated the potential NDVI that can be achieved due to land restoration and (2) we predicted the local surface temperature change of the NDVI increase using the relationships between NDVI and LST determined with the methods above.

As the maximum NDVI obtainable by land restoration depends on environmental conditions, we first predicted the NDVI that can potentially be achieved from land restoration in Africa, where we assumed that the potential NDVI is limited by the aridity index[69], land surface temperature (MOD11A1.061)[19], elevation, slope, aspect (SRTM90_V4)[81], soil fertility[82] and water table depth[83,84]. We thus considered only environmental and climatological constraints to vegetation rather than socio-economic constraints. We determined the relationship between NDVI and these variables based on 5000 random samples in the study area. After filtering for areas that are irrigated[85] or have a median NDVI lower than 0.15 (as the NDVI may be higher than can be expected based on natural conditions, or the points lay outside the study area), we divided the samples randomly into a training set (1840 samples) and a validation set (1839 samples). We used the training set to train a quantile regression forest[86] with 50 trees and 3 variables per tree. This was decided based on performance (visual inspection of the created map) and computation time. Quantile random forest fits the data to a percentile, in this case the 100-percentile, rather than the mean, representing the potential NDVI under the given environmental conditions[87]. We subtracted this median NDVI from the potential NDVI to create a map of potential NDVI increase (ΔNDVI) due to land restoration. If the predicted potential NDVI is lower than the current NDVI, the value was not changed. An evaluation of the random forest model is included in Supplementary Fig. 12, suggesting aridity to be the most important variable in predicting maximum NDVI.

To calculate the potential LST changes (ΔLST) from this ΔNDVI, we predicted the ΔLST across Africa using observed values of ΔLST and ΔNDVI and a random forest regression[88]. To this end, we sampled the observed maximum change in the NDVI trend component over the study period of the spatially corrected time series, as well as the related change in the LST trend component, at 3000 random points in each land cover class in the study area. We used the trend component instead of the 16-day component because we were interested in long-term changes in NDVI instead of the seasonal variability. Next, we filtered out random points with a median NDVI lower than 0.15. Using these methods, we created a training set (37,518 samples) and a validation set (5000 samples). The training set was used to train a random forest regression with 100 trees and 5 variables per tree, based on performance (highest correlation between observations and predicted values of the validation data set) and computation time. As predicting variables, we used the aridity index, land cover, median NDVI, median LST, median WSA (shortwave, visible and near-infrared), the NDVI–LST correlation of the trend component, latitude, longitude and altitude[81] as described in the input data. To then predict the potential LST change (ΔLST) related to land restoration, we ran the trained random forest model with the potential NDVI change (ΔNDVI) as input instead of the observed NDVI change. An evaluation of the random forest model is

included in Supplementary Fig. 13, showing a r^2 value of 0.83 and 0.53 for the training and validation data, respectively. The most important variables are the change in NDVI and the NDVI–LST correlation.

Data availability

MODIS NDVI (MOD13Q1.061), LST (MOD11A1.061), WSA (MCD43A3.006) and Land Cover (MCD12Q1) data are directly available through Google Earth Engine (https://developers.google.com/earth-engine/datasets), or can be downloaded from the NASA Earth Observing System Data and Information System (https://earthdata.nasa.gov/). Eddy covariance measurements are obtained from FLUXNET and available through (https://fluxnet.org/data/fluxnet2015-dataset/). WOCAT data is available through (https://www.wocat.net/en/). Data created in this study is available at https://doi.org/10.6084/m9.figshare.24072723.

Code availability

Google Earth Engine scripts are available at: https://code.earthengine.google.com/5deb2d58430918d3b6d14a1ed6481891 Other (Python) scripts and tiff are available at files: https://doi.org/10.6084/m9.figshare.24072723.

Received: 13 October 2023; Accepted: 27 August 2024;
Published online: 10 September 2024

References

1. Brancalion, P. H. & Holl, K. D. Guidance for successful tree planting initiatives. *J. Appl. Ecol.* **57**, 2349–2361 (2020).
2. Holl, K. *Primer of Ecological Restoration* (Island Press, 2020).
3. Shevliakova, E. et al. Historical warming reduced due to enhanced land carbon uptake. *Proc. Natl Acad. Sci. USA* **110**, 16730–16735 (2013).
4. Mahmood, R. et al. Land cover changes and their biogeophysical effects on climate. *Int. J. Climatol.* **34**, 929–953 (2014).
5. Bastin, J.-F. et al. The global tree restoration potential. *Science* **365**, 76–79 (2019).
6. Friedlingstein, P. et al. Global carbon budget 2020. *Earth Syst. Sci. Data* **12**, 3269–3340 (2020).
7. Martin, M. P. et al. People plant trees for utility more often than for biodiversity or carbon. *Biol. Conserv.* **261**, 109224 (2021).
8. Dhakal, S. et al. Emissions trends and drivers. In *Climate Change 2022: Mitigation of Climate Change. Contribution of Working Group III to the Sixth Assessment Report of the Intergovernmental Panel on Climate Change* (eds Shukla, P. R. et al.) (Cambridge University Press, 2022).
9. Ranasinghe, R. et al. Climate change information for regional impact and for risk assessment. In *Climate Change 2021: The Physical Science Basis. Contribution of Working Group I to the Sixth Assessment Report of the Intergovernmental Panel on Climate Change* (eds Masson-Delmotte, V. et al.) 1767–1926 (Cambridge University Press, 2021).
10. Engdaw, M. M., Ballinger, A. P., Hegerl, G. C. & Steiner, A. K. Changes in temperature and heat waves over Africa using observational and reanalysis data sets. *Int. J. Climatol.* **42**, 1165–1180 (2022).
11. Trisos, C. H. et al. Africa. In *Climate Change 2022: Impacts, Adaptation, and Vulnerability. Contribution of Working Group II to the Sixth Assessment Report of the Intergovernmental Panel on Climate Change* (eds Pörtner, H. O. et al.) 1285–1455 (Cambridge University Press, Cambridge, 2022).
12. Williams, P. A., Simpson, N. P., Totin, E., North, M. A. & Trisos, C. H. Feasibility assessment of climate change adaptation options across Africa: an evidence-based review. *Environ. Res. Lett.* **16**, 073004 (2021).
13. Ruijsch, J., Teuling, A. J., Verbesselt, J. & Hutjes, R. W. A. Landscape restoration and greening in Africa. *Environ. Res. Lett.* **18**, 064020 (2023).
14. Castelli, G., Castelli, F. & Bresci, E. Mesoclimate regulation induced by landscape restoration and water harvesting in agroecosystems of the horn of Africa. *Agric. Ecosyst. Environ.* **275**, 54–64 (2019).
15. Piao, S. et al. Characteristics, drivers and feedbacks of global greening. *Nat. Rev. Earth Environ.* **1**, 14–27 (2020).
16. Wolff, N. H., Masuda, Y. J., Meijaard, E., Wells, J. A. & Game, E. T. Impacts of tropical deforestation on local temperature and human well-being perceptions. *Glob. Environ. Change* **52**, 181–189 (2018).
17. Bennett, B. M. & Barton, G. A. The enduring link between forest cover and rainfall: a historical perspective on science and policy discussions. *For. Ecosyst.* **5**, 1–9 (2018).
18. Breil, M., Krawczyk, F. & Pinto, J. G. The response of the regional longwave radiation balance and climate system in Europe to an idealized afforestation experiment. *Earth Syst. Dyn.* **14**, 243–253 (2023).
19. Wan, Z., Hook, S. & Hulley, G. *MODIS/Terra Land Surface Temperature/Emissivity Daily L3 Global 1 km SIN Grid V061 [Dataset]* (NASA EOSDIS Land Processes Distributed Active Archive Center, 2021).
20. Betts, R. A. Offset of the potential carbon sink from boreal forestation by decreases in surface albedo. *Nature* **408**, 187–190 (2000).
21. Bonan, G. B. Forests and climate change: forcings, feedbacks, and the climate benefits of forests. *Science* **320**, 1444–1449 (2008).
22. Zeng, Z. et al. Climate mitigation from vegetation biophysical feedbacks during the past three decades. *Nat. Clim. Change* **7**, 432–436 (2017).
23. Bonan, G. B. Forests, climate, and public policy: A 500-year interdisciplinary odyssey. *Annu. Rev. Ecol. Evol. Syst.* **47**, 97–121 (2016).
24. Feldman, A. F. et al. Tropical surface temperature response to vegetation cover changes and the role of drylands. *Glob. Change Biol.* **29**, 110–125 (2022).
25. Chen, C. et al. Biophysical impacts of Earth greening largely controlled by aerodynamic resistance. *Sci. Adv.* **6**, eabb1981 (2020).
26. Spracklen, D., Baker, J., Garcia-Carreras, L. & Marsham, J. The effects of tropical vegetation on rainfall. *Annu. Rev. Environ. Resour.* **43**, 193–218 (2018).
27. Teuling, A. J. et al. Observational evidence for cloud cover enhancement over western European forests. *Nat. Commun.* **8**, 1–7 (2017).
28. Perugini, L. et al. Biophysical effects on temperature and precipitation due to land cover change. *Environ. Res. Lett.* **12**, 053002 (2017).
29. Li, Y. et al. Local cooling and warming effects of forests based on satellite observations. *Nat. Commun.* **6**, 1–8 (2015).
30. Pitman, A. et al. Importance of background climate in determining impact of land-cover change on regional climate. *Nat. Clim. Change* **1**, 472–475 (2011).
31. Teuling, A. J. et al. Contrasting response of European forest and grassland energy exchange to heatwaves. *Nat. Geosci.* **3**, 722–727 (2010).
32. Chen, C. et al. The biophysical impacts of idealized afforestation on surface temperature in China: local and nonlocal effects. *J. Clim.* **35**, 4233–4252 (2022).
33. Winckler, J., Lejeune, Q., Reick, C. H. & Pongratz, J. Nonlocal effects dominate the global mean surface temperature response to the biogeophysical effects of deforestation. *Geophys. Res. Lett.* **46**, 745–755 (2019).
34. Prevedello, J. A., Winck, G. R., Weber, M. M., Nichols, E. & Sinervo, B. Impacts of forestation and deforestation on local temperature across the globe. *PLoS ONE* **14**, e0213368 (2019).
35. Hoek van Dijke, A. J. et al. Shifts in regional water availability due to global tree restoration. *Nat. Geosci.* **15**, 363–368 (2022).
36. Duveiller, G., Hooker, J. & Cescatti, A. The mark of vegetation change on Earth's surface energy balance. *Nat. Commun.* **9**, 679 (2018).

37. Parr, C. L., te Beest, M. & Stevens, N. Conflation of reforestation with restoration is widespread. *Science* **383**, 698–701 (2024).
38. UNCCD. *Global Land Outlook* 2nd edn (UNCCD, 2022).
39. Hamunyela, E., Verbesselt, J. & Herold, M. Using spatial context to improve early detection of deforestation from Landsat time series. *Remote Sens. Environ.* **172**, 126–138 (2016).
40. Lhermitte, S., Verbesselt, J., Verstraeten, W. W. & Coppin, P. A pixel based regeneration index using time series similarity and spatial context. *Photogramm. Eng. Remote Sens.* **76**, 673–682 (2010).
41. Hackländer, J. et al. Land potential assessment and trend-analysis using 2000–2021 FAPAR monthly time-series at 250 m spatial resolution. *Peer J* **12**, e16972 (2024).
42. Vancutsem, C., Ceccato, P., Dinku, T. & Connor, S. J. Evaluation of MODIS land surface temperature data to estimate air temperature in different ecosystems over Africa. *Remote Sens. Environ.* **114**, 449–465 (2010).
43. Alkama, R. & Cescatti, A. Biophysical climate impacts of recent changes in global forest cover. *Science* **351**, 600–604 (2016).
44. Allen, S., Wallace, J., Gash, J. & Sivakumar, M. Measurements of albedo variation over natural vegetation in the Sahel. *Int. J. Climatol.* **14**, 625–636 (1994).
45. Yang, J., Li, Z., Zhai, P., Zhao, Y. & Gao, X. The influence of soil moisture and solar altitude on surface spectral albedo in arid area. *Environ. Res. Lett.* **15**, 035010 (2020).
46. Cordero, R. R. et al. Evaluation of MODIS-derived estimates of the albedo over the Atacama Desert using ground-based spectral measurements. *Sci. Rep.* **11**, 19822 (2021).
47. Liu, J. et al. Validation of moderate resolution imaging spectroradiometer (MODIS) albedo retrieval algorithm: Dependence of albedo on solar zenith angle. *J. Geophys. Res.: Atmos.* **114**, D01106 (2009).
48. Li, S. et al. Seasonality of albedo and fraction of absorbed photosynthetically active radiation in the temperate secondary forest ecosystem: A comprehensive observation using Qingyuan Ker towers. *Agric. For. Meteorol.* **333**, 109418 (2023).
49. Liang, S., Strahler, A. H. & Walthall, C. Retrieval of land surface albedo from satellite observations: a simulation study. *J. Appl. Meteorol.* **38**, 712–725 (1999).
50. Alibakhshi, S., Naimi, B., Hovi, A., Crowther, T. W. & Rautiainen, M. Quantitative analysis of the links between forest structure and land surface albedo on a global scale. *Remote Sens. Environ.* **246**, 111854 (2020).
51. Zheng, L. et al. Spatial, temporal, and spectral variations in albedo due to vegetation changes in China's grasslands. *ISPRS J. Photogramm. Remote Sens.* **152**, 1–12 (2019).
52. Hammerle, A., Haslwanter, A., Tappeiner, U., Cernusca, A. & Wohlfahrt, G. Leaf area controls on energy partitioning of a temperate mountain grassland. *Biogeosciences* **5**, 421–431 (2008).
53. Williamson, S. N., Barrio, I. C., Hik, D. S. & Gamon, J. A. Phenology and species determine growing-season albedo increase at the altitudinal limit of shrub growth in the sub-Arctic. *Glob. Change Biol.* **22**, 3621–3631 (2016).
54. Roy, D. P., Boschetti, L., Justice, C. & Ju, J. The collection 5 MODIS burned area product—Global evaluation by comparison with the MODIS active fire product. *Remote Sens. Environ.* **112**, 3690–3707 (2008).
55. Dintwe, K., Okin, G. S. & Xue, Y. Fire-induced albedo change and surface radiative forcing in sub-Saharan Africa savanna ecosystems: implications for the energy balance. *J. Geophys. Res.: Atmos.* **122**, 6186–6201 (2017).
56. Gatebe, C., Ichoku, C., Poudyal, R., Román, M. & Wilcox, E. Surface albedo darkening from wildfires in northern sub-Saharan Africa. *Environ. Res. Lett.* **9**, 065003 (2014).
57. Abiodun, B. J., Adeyewa, Z. D., Oguntunde, P. G., Salami, A. T. & Ajayi, V. O. Modeling the impacts of reforestation on future climate in West Africa. *Theor. Appl. Climatol.* **110**, 77–96 (2012).
58. Davin, E. L., & de Noblet-Ducoudré, N. Climatic impact of global-scale deforestation: radiative versus nonradiative processes. *J. Clim.* **23**, 97–112 (2010).
59. Akkermans, T., Thiery, W. & Van Lipzig, N. P. M. The regional climate impact of a realistic future deforestation scenario in the Congo basin. *J. Clim.* **27**, 2714–2734 (2014).
60. Duveiller, G. et al. Local biophysical effects of land use and land cover change: towards an assessment tool for policy makers. *Land Use Policy* **91**, 104382 (2020).
61. Huete, A. R., HuiQing, L. & van Leeuwen, W. J. D. The use of vegetation indices in forested regions: issues of linearity and saturation. In *IGARSS'97. 1997 IEEE International Geoscience and Remote Sensing Symposium Proceedings. Remote Sensing—A Scientific Vision for Sustainable Development,* **4**, 1966–1968 (Singapore, 1997).
62. UNCCD. *The Great Green Wall Implementation Status and Way Ahead to 2030* (UNCCD, 2020).
63. Holl, K. D. & Brancalion, P. H. Tree planting is not a simple solution. *Science* **368**, 580–581 (2020).
64. Gorelick, N. et al. Google Earth engine: planetary-scale geospatial analysis for everyone. *Remote Sens. Environ.* **202**, 18–27 (2017).
65. Didan, K. *MODIS/Terra Vegetation Indices 16-Day L3 Global 250 m SIN Grid V061 [Dataset]* (NASA EOSDIS Land Processes Distributed Active Archive Center, 2021).
66. Schaaf, C. & Wang, Z. *MCD43A3 MODIS/Terra+Aqua BRDF/Albedo Daily L3 Global—500 m V006 [Dataset]* (NASA EOSDIS Land Processes Distributed Active Archive Center, 2015).
67. Sulla-Menashe, D., Gray, J. M., Abercrombie, S. P. & Friedl, M. A. Hierarchical mapping of annual global land cover 2001 to present: The MODIS Collection 6 Land Cover product. *Remote Sens. Environ.* **222**, 183–194 (2019).
68. Cherlet, M. et al. *World Atlas of Desertification*. 3rd edn (Publication Office of the European Union, 2018).
69. Zomer, R. J., Xu, J. & Trabucco, A. Version 3 of the global aridity index and potential evapotranspiration database. *Sci. Data* **9**, 409 (2022).
70. Middleton, N. & Thomas, D. *World Atlas of Desertification* 2nd edn (United Nations Environment Program, 1997).
71. Verbesselt, J., Hyndman, R., Newnham, G. & Culvenor, D. Detecting trend and seasonal changes in satellite image time series. *Remote Sens. Environ.* **114**, 106–115 (2010).
72. Verbesselt, J., Hyndman, R., Zeileis, A. & Culvenor, D. Phenological change detection while accounting for abrupt and gradual trends in satellite image time series. *Remote Sens. Environ.* **114**, 2970–2980 (2010).
73. Verbesselt, J., Zeileis, A. & Herold, M. Near real-time disturbance detection using satellite image time series. *Remote Sens. Environ.* **123**, 98–108 (2012).
74. Hamunyela, E. et al. Implementation of BFASTmonitor algorithm on Google Earth engine to support large-area and sub-annual change monitoring using earth observation data. *Remote Sens.* **12**, 2953 (2020).
75. Ardö, J., Mölder, M., El-Tahir, B. A. & Elkhidir, H. A. M. Seasonal variation of carbon fluxes in a sparse savanna in semi arid Sudan. *Carbon Balance Manag.* **3**, 1–18 (2008).
76. Tagesson, T. et al. Ecosystem properties of semiarid savanna grassland in West Africa and its relationship with environmental variability. *Glob. Change Biol.* **21**, 250–264 (2015).
77. Archibald, S. et al. Drivers of inter-annual variability in net ecosystem exchange in a semi-arid savanna ecosystem, South Africa. *Biogeosciences* **6**, 251–266 (2009).
78. Merbold, L. et al. Precipitation as driver of carbon fluxes in 11 African ecosystems. *Biogeosciences* **6**, 1027–1041 (2009).
79. Chiti, T., Certini, G., Grieco, E. & Valentini, R. The role of soil in storing carbon in tropical rainforests: the case of Ankasa Park, Ghana. *Plant Soil* **331**, 453–461 (2010).

80. WOCAT. *Global Sustainable Land Management Database* (World Overview of Conservation Approaches and Technologies, 2022).
81. Reuter, H. I., Nelson, A. & Jarvis, A. An evaluation of void-filling interpolation methods for SRTM data. *Int. J. Geogr. Inf. Sci.* **21**, 983–1008 (2007).
82. Hengl, T. et al. African soil properties and nutrients mapped at 30 m spatial resolution using two-scale ensemble machine learning. *Sci. Rep.* **11**, 6130 (2021).
83. Fan, Y., Li, H. & Miguez-Macho, G. Global patterns of groundwater table depth. *Science* **339**, 940–943 (2013).
84. Fan, Y., Miguez-Macho, G., Jobbágy, E. G., Jackson, R. B. & Otero-Casal, C. Hydrologic regulation of plant rooting depth. *Proc. Natl Acad. Sci. USA* **114**, 10572–10577 (2017).
85. Meier, J., Zabel, F. & Mauser, W. A global approach to estimate irrigated areas—a comparison between different data and statistics. *Hydrol. Earth Syst. Sci.* **22**, 1119–1133 (2018).
86. Meinshausen, N. & Ridgeway, G. Quantile regression forests. *J. Mach. Learn. Res.* **7**, 983–999 (2006).
87. Roebroek, C. T., Duveiller, G., Seneviratne, S. I., Davin, E. L. & Cescatti, A. Releasing global forests from human management: how much more carbon could be stored? *Science* **380**, 749–753 (2023).
88. Breiman, L. Random forests. *Mach. Learn.* **45**, 5–32 (2001).

Acknowledgements

The authors gratefully thank the Africa Water Foundation for funding this research. We also like to acknowledge the reviewers, who critically reviewed several versions of this manuscript. We believe that implementing the comments considerably improved this research.

Author contributions

J.R. designed the research, performed the research, contributed new analytic tools, analysed the data, and wrote the paper. A.J.T. designed the research, analysed the data and wrote the paper. G.D. analysed the data and wrote the paper. R.W.A.H. designed the research, analysed the data and wrote the paper.

Competing interests

The authors declare no competing interests.

Additional information

Supplementary information The online version contains supplementary material available at https://doi.org/10.1038/s43247-024-01650-x.

Correspondence and requests for materials should be addressed to Jessica Ruijsch or Adriaan J. Teuling.

Peer review information *Communications Earth & Environment* thanks Temesgen Alemayehu Abera, Jörg Kaduk and the other, anonymous, reviewer(s) for their contribution to the peer review of this work. Primary Handling Editors: Erika Buscardo, Aliénor Lavergne, and Carolina Ortiz Guerrero. A peer review file is available.